Identification of twinned gas phase clusters by single-shot scattering with intense soft x-ray pulses

2012 New J. Phys. 14 055016

(http://iopscience.iop.org/1367-2630/14/5/055016)

New Journal of Physics
The open-access journal for physics

Identification of twinned gas phase clusters by single-shot scattering with intense soft x-ray pulses

D Rupp[1,9], M Adolph[1], T Gorkhover[1], S Schorb[1,2], D Wolter[1], R Hartmann[3], N Kimmel[4,5], C Reich[3], T Feigl[6], A R B de Castro[7], R Treusch[8], L Strüder[4,5], T Möller[1] and C Bostedt[1,2]

[1] Institut für Optik und Atomare Physik, Technische Universität Berlin, Hardenbergstraße 36, 10623 Berlin, Germany
[2] SLAC National Accelerator Laboratory, 2575 Sand Hill Road, Menlo Park, CA 94025, USA
[3] PNSensor GmbH, Otto-Hahn-Ring 6, 81739 München, Germany
[4] Max-Planck-Institut Halbleiterlabor, Otto-Hahn-Ring 6, 81739 München, Germany
[5] Max-Planck-Institut für extraterrestrische Physik, Gießenbachstraße, 85741 Garching, Germany
[6] Fraunhofer-Institut für Angewandte Optik und Feinmechanik, Albert-Einstein-Straße 7, 07745 Jena, Germany
[7] Instituto de Fisica Gleb Wataghin, Universidade Estadual de Campinas, 13083-970, Campinas, Brazil
[8] Deutsches Elektronen-Synchrotron DESY, Notkestraße 85, 22603 Hamburg, Germany
E-mail: daniela.rupp@physik.tu-berlin.de

New Journal of Physics **14** (2012) 055016 (11pp)
Received 30 January 2012
Published 16 May 2012
Online at http://www.njp.org/
doi:10.1088/1367-2630/14/5/055016

Abstract. Scattering experiments on xenon nanoclusters with high-intensity soft x-ray laser pulses from the **F**ree-Electron **LAS**er in **H**amburg (FLASH) are performed to investigate different cluster morphologies in the gas phase. Three different types of scattering patterns can be identified. The most frequent pattern of concentric rings reflects the event of a single spherical cluster in focus. Fine interference rings similar to Newton rings appear when two clusters are illuminated at μm distance, revealing three-dimensional information about the location of the clusters. Between 10 and 30% of all hits show a previously unknown twin cluster configuration with two clusters in direct

[9] Author to whom any correspondence should be addressed.

contact. Simulations of scattering patterns for twin clusters with different sizes of the two particles, degree of fusion and orientation in space allow us to explain all the observed patterns.

Contents

1. Introduction **2**
2. Experiment **3**
3. Results **4**
3.1. Overview 4
3.2. Concentric ring structures 5
3.3. Newton rings 6
3.4. Twin clusters 6
4. Simulations of twin clusters and Newton rings **7**
5. Summary and outlook **10**
Acknowledgments **11**
References **11**

1. Introduction

Free-electron lasers (FELs) with photon energies well into the hard x-ray regime enable a wide range of novel experiments [1]. Within this development, single-shot imaging of free particles in the gas phase [2–4] and in particular of non-repetitive biological objects has become possible [5]. According to detailed theoretical studies, the achievable spatial resolution for structure determination in such experiments is ultimately limited by radiation damage [6–8]. Hence, understanding of underlying processes such as ionization and fragmentation is of key interest for all kinds of imaging applications. The investigation of simple model systems such as rare gas clusters in the gas phase with intense short light pulses helps one to gain deep insight into the light–matter interaction [3, 9]. The novel method of single-shot single-particle imaging opens the door for a new class of experiments. From the scattering patterns of single-clusters, both structure and transient changes in the electronic properties of the particles due to the interaction with light can be extracted. Therefore, radiation damage on the timescale of femtoseconds can be followed by x-ray scattering on single spherical xenon clusters [10].

In this paper, we focus on the analysis of the structural information contained in the scattering patterns of a single or a few clusters. We demonstrate that three-dimensional (3D) information can be extracted from the scattering patterns of two spherical clusters in the x-ray focus. Further, we show that the shape of rare gas clusters can significantly differ from the most frequent case of a sphere. The scattering patterns of single particles contain a very high percentage of double cluster structures. In principle, such 'twin clusters' are predicted to appear as intermediate states in the cluster growth process [11]. However, so far it has not been observed that non-spherical objects can freeze out in the gas phase and be detected milliseconds after the expansion [12]. These new findings on cluster morphology extend the model character of rare gas clusters to the investigation of both spherical and non-spherical systems. By modeling a large array of cluster geometries we show that the scattering patterns allow us to distinguish various 2D and 3D cluster configurations.

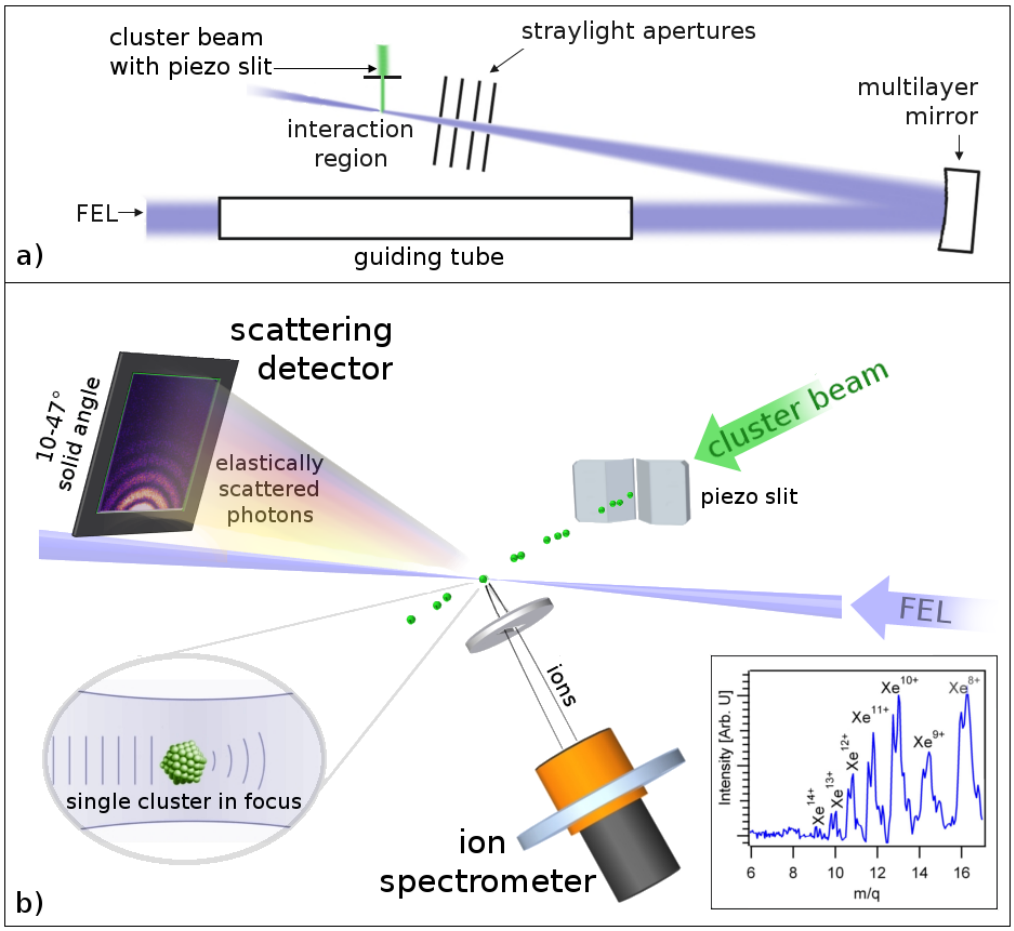

Figure 1. (a) Optical path of the experimental layout: a guiding tube for the incoming beam and a multilayer-based off-axis backfocusing geometry allow for quasi background-free scattering measurements. (b) Schematic layout of the interaction region: a cluster beam is skimmed down to one cluster in the focal volume by a piezo slit. The micrometer focal spot is optimized using a time-of-flight ion spectrometer. By moving the multilayer mirror along the bisecting line between the incoming and focused FEL beams, we can scan on power density-dependent nonlinear processes in xenon ion spectra (displayed for highest power density in the inset). A fast readout pnCCD detector [13, 14] measures the elastically scattered photons from single xenon clusters.

2. Experiment

For the studies of this paper, a new experimental setup for the single-shot imaging of nanometer-sized samples at the **F**ree-Electron **LAS**er in **H**amburg (FLASH) was designed combining a spectroscopy approach and an imaging approach. The experiment was performed at the unfocused beamline BL3 by using 20 fs pulses with about 10^{12} photons of 92 eV photon energy [15]. The optical path is given in figure 1(a) and a schematic layout of the interaction region is presented in figure 1(b).

The soft x-ray pulses are focused by a multilayer mirror into a focal spot of about five microns diameter (full-width at half-maximum). We use an off-axis backfocusing geometry with an angle of 2.5° between the incident and reflected beams in order to cover small scattering angles without blocking the incoming beam. Additionally, by using this geometry the incoming beam does not cross the interaction region, which greatly reduces the background from the fluorescent light.

The cluster beam is generated by supersonic expansion of xenon through a cryogenically cooled and pulsed conical nozzle with a diameter of 200 μm and a half-cone angle of 4°. The cluster beam is guided into the differentially pumped main chamber through a conical skimmer with an opening diameter of 1 mm. The cluster size can be controlled by adjusting the temperature and gas pressure [16]. To achieve the 'single-cluster mode' where fewer than one cluster at a time is in the focal volume, the cluster beam can be further skimmed down by an additional movable piezoelectric driven skimmer slit with an adjustable width between 0 and 1.5 mm. Single-cluster mode settings have to be found for all pressure and temperature settings, as the number of clusters per volume depends on the expansion parameters, specifically on the generated cluster size in relation to the stagnation pressure [16, 17].

An implemented time-of-flight spectrometer with an entrance aperture comparable to the Rayleigh length of the FEL focus is used to characterize the FEL focus and find perfect overlap of the laser and the cluster beam at the highest power densities. By moving the multilayer mirror we scan along the FEL beam axis on power-density-dependent nonlinear processes in xenon ion spectra. At an FEL pulse energy of 30 μJ, xenon charge states up to 14^+ are detected (inset of figure 1(b)) corresponding to a power density of $\approx 2 \times 10^{15}\,\mathrm{W\,cm^{-2}}$ [18].

Elastically scattered photons are detected by a set of novel high-performance pnCCD detectors, which are ideal for soft x-ray imaging applications thanks to their linear response, low noise and fast readout [13, 14]. The active chip size of the detectors is $(20\,\mathrm{mm})^2$ with a pixel size of $(75\,\mu\mathrm{m})^2$. By an optimized assembling of three detectors around the interaction region, a large scattering angle from 10° to 128° is covered. Only the detector at the smallest scattering angles of 10–47° is shown in figure 1 as the analysis in the present paper addresses only patterns measured by this detector. The achievable resolution of the setup is limited by the highest momentum transfer q that can be detected. With the scattering detector covering angles up to 47°, a maximal detectable momentum transfer of $q = 4\pi/\lambda \cdot \sin(\theta/2) = 0.36\,\mathrm{nm^{-1}}$ limits the resolution to $2\pi/q = 17$ nm.

3. Results

3.1. Overview

Single xenon clusters with radii from ≈100 nm down to 25 nm were imaged using the setup described above. In general, three categories of structures can be identified in the recorded scattering patterns: clean single-cluster patterns with beam-concentric ring structures, patterns superimposed with a fine eccentric ring structure and double-slit-like patterns. Examples of each category are displayed in figures 2(b)–(d). First, a statistical analysis is presented on the basis of a data set of 500 scattering patterns taken at a stagnation pressure of 14 bar xenon gas at 220 K and a piezo skimmer slit width of 0.5 mm. In figure 2(a), the average number of photons per pixel on the CCD detector is plotted for every pulse of this data set. Only 34 bright patterns out of 500 shots peak out of the background noise (7% hits), clearly indicating single-cluster

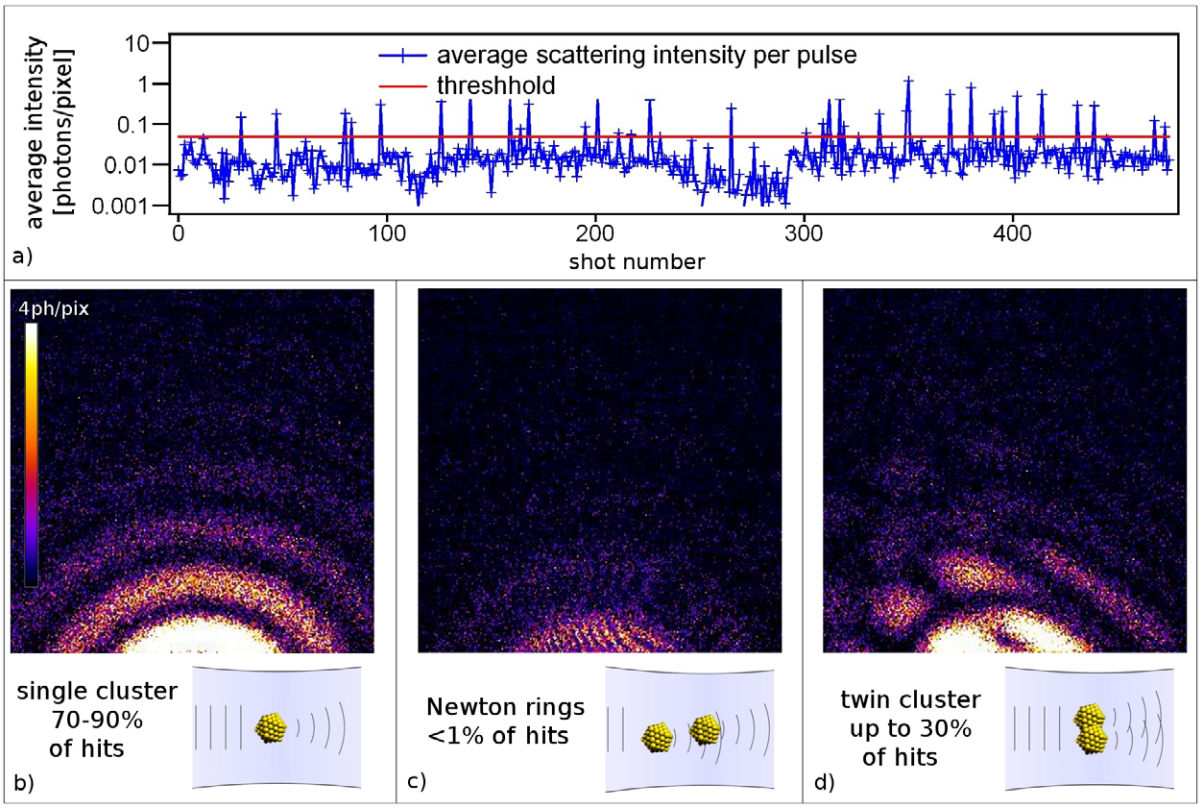

Figure 2. (a) The average scattered light per pulse in an exemplary data set of 500 shots indicates single-cluster mode. (b) In ≈ 70–90% of all hits, the expected ring structure of a spherical particle is found. (c) In less than 1% of all hits, 'Newton rings' appear, indicating two clusters in a line at micrometer distance. (d) Previously unknown non-spherical structures of 'Twin clusters' are found in up to 30% of all hits.

mode. The threshold to discriminate between an event and background noise (expressed by the red line in figure 2(a)) was set to 0.05 scattered photon per pixel, which is clearly above the noise level (7σ). The following discussion focuses on analysis of the observed scattering patterns by comparing them with the simulated scattering patterns calculated from assumed geometries. An in-depth investigation of the influence of expansion parameter settings on the cluster morphology and the implications of our findings for cluster growth processes will be discussed in detail elsewhere [12].

3.2. Concentric ring structures

The majority of the recorded scattering patterns exhibit concentric ring structures (see figure 2(b)), representing single-clusters in the focus. Within the resolution limits given in section 2 these clusters are spherical. However, the scattering patterns of much bigger clusters ($R \approx 150$ nm) taken with higher resolution [10] show intensity fluctuations within the outermost rings which might be indications of surface facets. Such ring structures as in figure 2(b) appear

23 times in 34 hits, adding up to 67% of all hits. With simulations based on Mie's theory [19, 20], intensity profiles of the patterns can be fitted determining the particle size and the refractive index as the corresponding parameter to the excited electronic state of the cluster. During the interaction with the intense x-ray pulse the electronic structure of the particle is altered, leaving distinct fingerprints on the scattering pattern [10]. In order to obtain accurate information from the Mie calculations, both the size and the optical constants were used as fitting parameters. The deviation from radii fitted using the optical constants of neutral xenon is less than 2 nm (about 4%). The average cluster radius of $R = 51$ nm, obtained from those 23 patterns, is in good agreement with scaling laws [16], which predict a radius of 53 nm.

3.3. Newton rings

A much rarer but recurrent pattern is fine interference fringes akin to Newton rings. Examples are displayed in figures 2(c) and 3(d). When two clusters are illuminated at a certain distance as discussed in further detail below, Newton rings superimpose the basic scattering pattern alongside the axis that intersects both clusters. These Newton rings allow us to extract real 3D structural information out of a single scattering pattern as the center of the Newton rings represents the orientation of the cluster axis with respect to the incoming beam, while the separation of both clusters can be determined from the distance of the fringes.

The appearance of Newton rings is expected from statistical considerations. Although the vast majority of all pulses intercept no target or a single-cluster, with a small probability two clusters are hit in the focal volume. It is important to note that we detect only a part of those events with two clusters in a line for two reasons. Firstly, the fine structure can only be seen if the cluster axis comes close to or intersects the scattering detector which covers only a small solid angle. Secondly, two clusters' scattering waves can only interfere if the path difference for the scattered light from both clusters remains within the coherence length of the FEL. The coherence time of FLASH of 4.2 fs [15] allows a path difference for the scattered light of 1.3 μm. This limits the observation of Newton rings either to small angles between the cluster axis and FEL beam or short distance between both clusters, respectively. Over all the recorded data ($\sim 10^4$ patterns) the occurrence probability for Newton rings was 0.01–1% of hits, depending on expansion parameters and skimmer slit opening, i.e. the cluster density in the focal volume. Simulations of the patterns as discussed below revealed cluster separations between 5 and 20 μm. In agreement with a maximal path difference of 1.3 μm the center of the rings always appeared at small scattering angles ($\approx$ 10–25°).

3.4. Twin clusters

Twin clusters similar to the example displayed in figure 2(d) have not been observed in previous gas phase experiments as the more conventionally used methods such as mass spectrometry are not sensitive to the object shape. Only single-shot imaging techniques can uncover their presence. Our findings reveal not only the presence of such non-spherical configurations but also a surprisingly high incidence. Within the 34 hits presented in figure 2(a), 7 twin patterns were observed. Over all the data, about 10–30% of all hits show twin clusters similar to the pattern in figure 2(d). The development of cluster size distributions with changing expansion parameters and the abundance of twin clusters has been analyzed in a detailed study elsewhere [12].

The simulations of the scattering patterns discussed below clearly support the conclusion that the clusters are twin structures. But also from statistical considerations it can be excluded

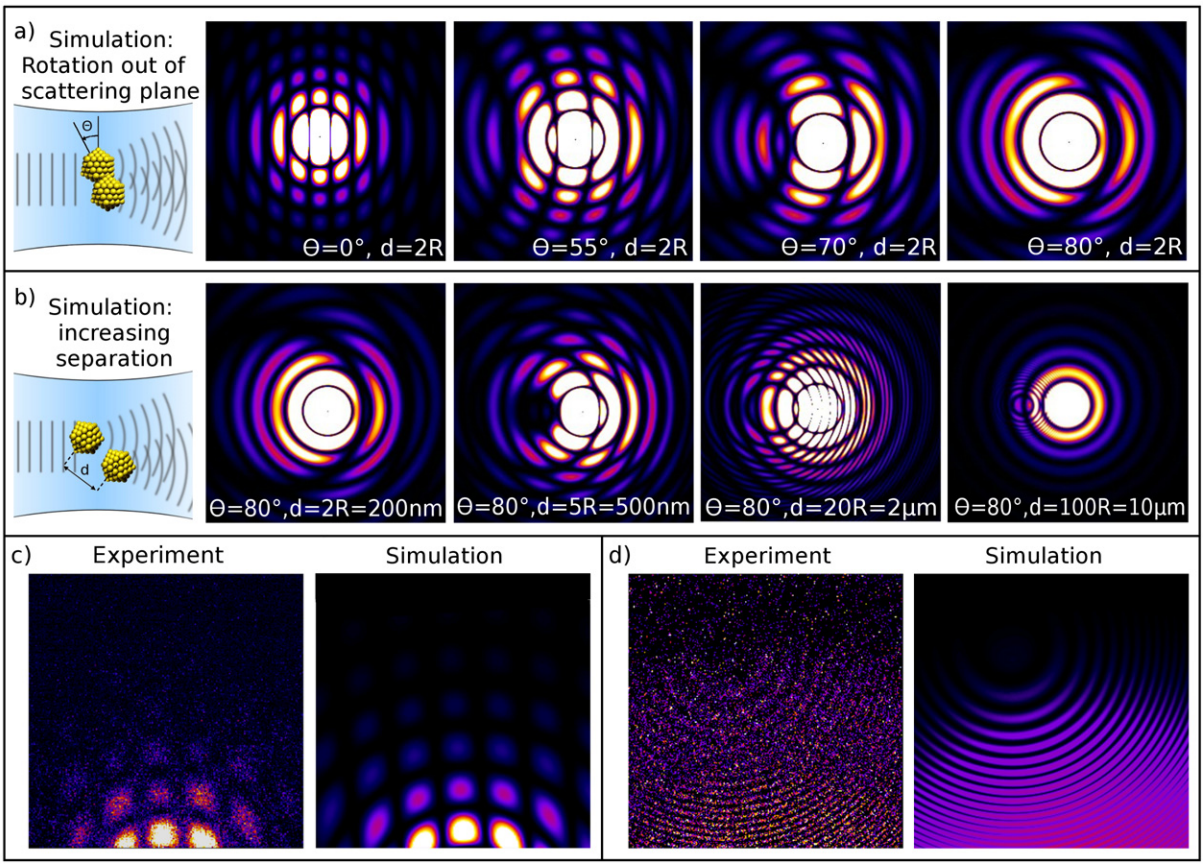

Figure 3. Simulations for two equally sized clusters (a) in contact and rotated out of the scattering plane and (b) at a fixed angle of 80° with increasing separation. Calculations are done with an adaption of the program ClusScat3 [22]. (c) The typical obtained pattern of the 'classical double slit' case can be explained by two similarly sized clusters in direct contact ($R = 65$ nm at 130 nm distance). (d) The typical 'Newton rings' pattern is in good agreement with simulations for one cluster after the other with a 10 μm separation and an axis rotation of 22° (see footnote 10).

that the patterns result from two separate clusters which are coincidentally close: in single-particle mode, the probability of finding two separate clusters within a distance <100 nm can be deduced from the typical distance between the two clusters of about 10 μm found in scattering patterns with Newton rings. The ratio of their cubic volumes $(100\,\text{nm})^3/(10\,\mu\text{m})^3 = 10^{-6}$ gives an upper limit.

4. Simulations of twin clusters and Newton rings

To discuss the trends developing in the diffraction patterns, we have simulated distinct scenarios for the interpretation of the data, rather than relying on reconstruction codes. As was demonstrated recently, a reconstruction of scattering patterns can provide detailed information on the shape of a particle [4, 5, 21]. Reconstructions of single patterns yield 2D projections of the particles and are therefore not applicable to patterns with Newton rings.

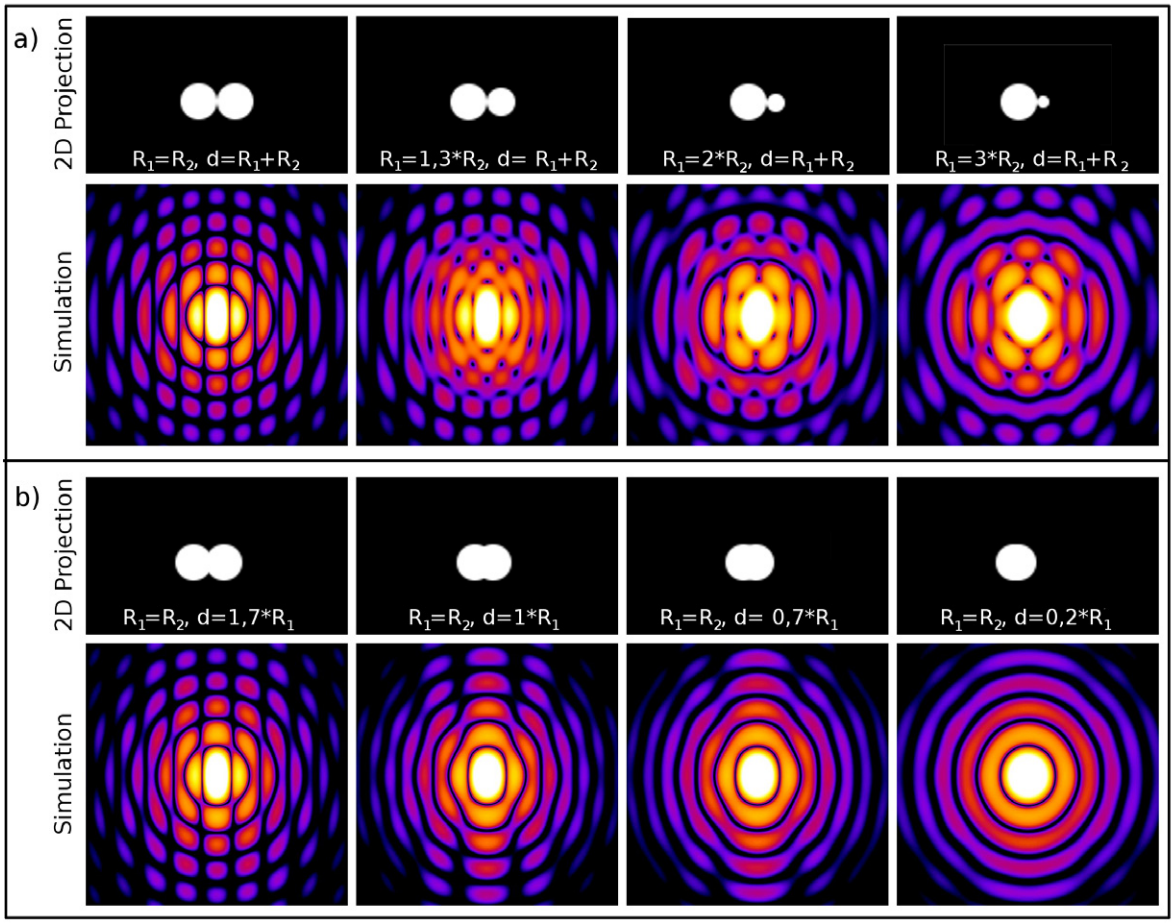

Figure 4. Simulations for (a) two clusters in contact with shrinking size of the second cluster and (b) two equally sized clusters with shrinking distance. The simulated patterns are obtained by Fourier transform of 2D projections as displayed in the first and third rows.

Simulated patterns are calculated from estimated 3D and 2D structures and compared to the experimental data. By taking into account a variety of parameters and by careful comparison with the measured scattering patterns, cluster configurations can be determined. Virtually all detected patterns can be explained by simulations that allow for three degrees of freedom:

- the orientation of the two clusters with respect to the scattering plane (figure 3(a));
- the distance between two clusters, i.e. separation in the case of Newton rings (figure 3(b)) and fusion for twin clusters (figure 4(b));
- sizes of both the particles (figure 4(a)).

A numerical approach with a scalar approximation of the scattering process as described in [22] can be used to calculate scattering patterns for 3D configurations of two spherical particles. We used this approach for the cases when the spatial dimension or distribution of the scattering bodies along the beam axis plays an important role (figure 3). The simulated patterns shown in figure 3 are calculated with an adapted version of the program ClusScat3 [22].

Figure 3(a) displays the changes in the scattering pattern of two equally sized clusters in direct contact at a rotation out of the scattering plane of $\Theta = 0°,\ 55°, 70°$ and $80°$. The straight fringes of the double-slit-like pattern at $0°$ are bent until the dumbbell axis intersects the detector plane and reveals their nature as destructive interference rings around the cluster axis.

In the transition to Newton rings in figure 3(b) (the last pattern in figure 3(a) and the first pattern in figure 3(b) show the same case) this trend becomes even clearer. The increasing distance between the particle centers of equally sized particles with $R_1 = R_2 = 100\,\text{nm}$ at a fixed rotation angle of $\Theta = 80°$ from contact up to $10\,\mu\text{m}$ separation shrinks the distance between the fringes, making the interference structure finer. In our data we find images of the 'classical double slit' as well as Newton rings indicating a few micrometers distance (the left part of figures 3(c) and (d)). Simulations with $R_1 = R_2 = 65\,\text{nm}$ in direct contact for figure 3(c) and two $R_1 = R_2 = 22\,\text{nm}$ clusters at $10\,\mu\text{m}$ distance at a rotation of $68°$ for figure 3(d)[10] agree well with the recorded patterns. An error of about 5% is expected for the determined size ratios due to uncertainties within the fits. Note that for the absolute cluster sizes an additional error of about 4% has to be taken into account as the simulations neglect changes in the optical constants and resulting size deviations as described in section 3.2.

Scattering patterns of twin clusters which differ from the simple case of figure 3(c) can be simulated by allowing different radii $R_1 \neq R_2$ of the two particles and different degree of fusion, i.e. shrinking distance between the centers of the two particles $d < R_1 + R_2$. Simulations of examples for both the cases are displayed in figure 4.

Within the scattering plane, or for only a small rotation of the cluster axis out of the scattering plane, the structure of the patterns is given by the Fourier transformed 2D projection of the scatterer on the scattering plane. As figure 3(a) shows for the case of two equally sized clusters with $d = 2R$, even the alterations of the structures caused by a rotation of $55°$ consist primarily of a simple bending of the basic pattern. Accordingly, all trends which can be found in a 3D calculation as ClusScat3 [22] also occur in Fourier transformations of the 2D projection. Therefore the studies of varying particle sizes and distances were done by Fourier transforming black/white masks of the 2D projections which are shown in the first and third rows of figure 4. Still, configurations with $\Theta > 45°$ will certainly have to be calculated with a 3D simulation program such as ClusScat3.

The patterns in figure 4(a) are simulated for decreasing size of the second sphere ($R_1/R_2 = 1|1.3|2|3$) and in (b) for equally sized spheres of decreasing distance between the particle centers ($d = 1.7|1|0.7|0.2 \cdot R_1$). In the limit of (a) $R_2 \to 0$, respectively (b) $d \to 0$, both the cases end up in the well-known pattern of a single spherical cluster, i.e. ring structures as in figure 2(b). While approaching this limit, in both situations the clearly defined maxima and minima of the sidelobes tend to smear out. In the case of fusion this develops from the center to outer rings as can be followed in figure 4(b), where only the outer rings show clear substructures. In contrast, in the case of different sizes the substructure differs from ring to ring, depending on the size ratio of the two spheres and the subsequent interference. At a size ratio of $R_1/R_2 = 3$, displayed in the last simulation of figure 4(a), the third ring is rather homogeneous, whereas both higher and lower maxima, show a pronounced substructure.

A selection of experimental patterns is displayed in the first row of figure 5. A comparison with the simulated patterns shows that very good agreement can be obtained and that the fine

[10] The pattern displayed in figure 3(d) was recorded in a slightly different setup with a scattering detector placed at 70 mm distance covering a scattering angle of 11–27°.

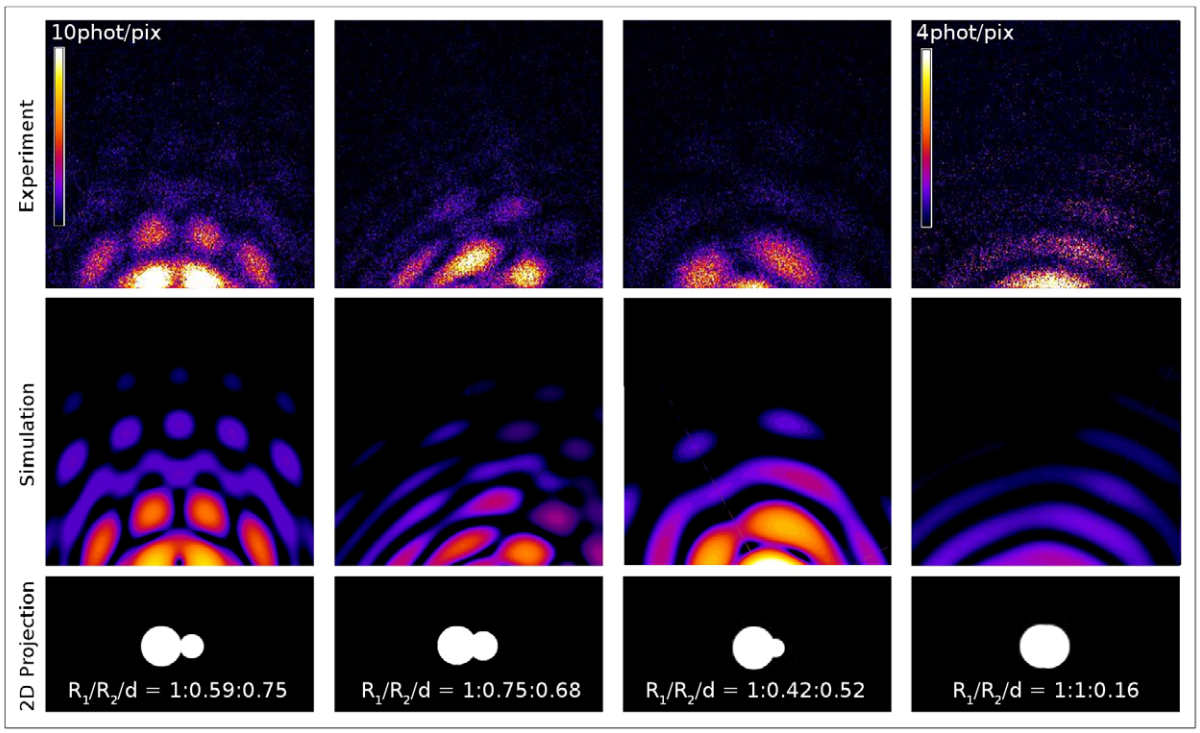

Figure 5. Snapshots of cluster morphology: a selection of typical experimental patterns (first row). Simulated patterns considering different sizes and degree of fusion are in good agreement (second row). Corresponding 2D projections with ratios of bigger radius to smaller radius to the distance between the centers (third row).

structure is reproduced when the size and degree of fusion are taken into account (middle row). The masks used for the Fourier transformations as well as the yielded parameters are displayed in the third row. The finding of various degrees of fusion from two clusters in direct contact with one slightly non-spherical structure indicates that interstages of the cluster growing process driven by coagulation of particles can freeze out and be detected milliseconds after the expansion [11, 12].

5. Summary and outlook

We have reported on the imaging of a single and a few xenon clusters with ultrashort soft x-ray pulses at the FLASH FEL. Information on geometric configurations and cluster morphology is extracted from the measured scattering patterns. The size and shape of single spherical clusters and full 3D information on the position and separation of two clusters in the case of 'Newton rings' are derived. A large fraction of scattering patterns show fringes which stem from twinned clusters. Simulations of the scattering patterns calculated from double structures with varying size, distance and orientation of both the clusters explain all the observed structures. Our findings will help shed light on the fundamental processes in the cluster growth process and answer long-standing questions about the coagulation of clusters in the gas phase. Further, in an extended setup with the simultaneous measurement of scattering patterns and ion or electron

spectra of single particles, unprecedented insight into the light–matter interaction in the x-ray regime can be obtained. By comparing non-spherical twin clusters to spherical single-clusters with the same number of atoms, the important role of the particle surface can be investigated.

Acknowledgments

We thank the members of the DESY staff and the IOAP workshop for their extraordinary support and M Müller for fruitful discussions. Funding by the Bundesministerium für Bildung und Forschung grants 05KS4KT1, 05KS7KT2 and 05K10KT2, the DFG grant BO 3169/2-2 and HGF Virtuelles Institut VH VI-302 is acknowledged.

References

[1] Bostedt C *et al* 2009 Experiments at FLASH *Nucl. Instrum. Methods Phys. Res.* A **601** 108–22
[2] Bogan M *et al* 2008 Single particle X-ray diffractive imaging *Nano Lett.* **8** 310–6
[3] Bostedt C *et al* 2010 Clusters in intense FLASH pulses: ultrafast ionization dynamics and electron emission studied with spectroscopic and scattering techniques *J. Phys. B: At. Mol. Opt. Phys.* **43** 194011
[4] Chapman H *et al* 2011 Femtosecond X-ray protein nanocrystallography *Nature* **470** 73–7
[5] Seibert M *et al* 2011 Single mimivirus particles intercepted and imaged with an X-ray laser *Nature* **470** 78–81
[6] Bergh M *et al* 2008 Feasibility of imaging living cells at subnanometer resolutions by ultrafast X-ray diffraction *Q. Rev. Biophys.* **41** 181–204
[7] Son S, Young L and Santra R 2011 Impact of hollow-atom formation on coherent x-ray scattering at high intensity *Phys. Rev.* A **83** 033402
[8] Neutze R *et al* 2000 Potential for biomolecular imaging with femtosecond x-ray pulses *Nature* **406** 752–7
[9] Saalmann U, Siedschlag Ch and Rost J M 2006 Mechanisms of cluster ionization in strong laser pulses *J. Phys. B: At. Mol. Opt. Phys.* **39** R39–77
[10] Bostedt C *et al* 2012 Ultrafast X-ray scattering of xenon nanoparticles: imaging transient states of matter *Phys. Rev. Lett.* **108** 093401
[11] Soler J M *et al* 1982 Microcluster growth: transition from successive monomer addition to coagulation *Phys. Rev. Lett.* **49** 1856–60
[12] Adolph M *et al* Imaging of single and twin rare gas clusters using intense soft x-ray pulses (in preparation)
[13] Meidinger N *et al* 2006 Next generation of pnCCDs for x-ray spectroscopy and imaging *Nucl. Instrum. Methods Phys. Res.* A **568** 141–8
[14] Strüder L *et al* 2010 Large-format, high-speed, x-ray pnCCDs combined with electron and ion imaging spectrometers in a multipurpose chamber for experiments at 4th generation light sources *Nucl. Instrum. Methods Phys. Res.* A **614** 483–96
[15] Ackermann W *et al* 2007 Operation of a free-electron laser from the extreme ultraviolet to the water window *Nature Photonics* **1** 336–42
[16] Hagena O F 1981 Nucleation and growth of clusters in expanding nozzle flows *Surf. Sci.* **106** 101–16
[17] Beijerinck H C W *et al* 1985 Campargue-type supersonic beam sources: absolute intensities, skimmer transmission and scaling laws for mono-atomic gases He, Ne and Ar *Chem. Phys.* **96** 153–73
[18] Sorokin A A *et al* 2007 Photoelectric effect at ultrahigh intensities *Phys. Rev. Lett.* **99** 213002
[19] Mie G 1908 Beiträge zur Optik trüber Medien, speziell kolloidaler Metallösungen *Ann. Phys.* **330** 377–445
[20] Bohren C F and Huffman D 1983 *Absorption and Scattering of Light by Small Particles* (New York: Wiley)
[21] Miao J, Charalambous P and Kirz J 1999 Extending the methodology of x-ray crystallography to allow imaging of micrometre-sized non-crystalline specimens *Nature* **400** 342–4
[22] de Castro A R B *et al* 2008 Numerical simulation of small angle scattering (SAXS) for large atomic clusters *J. Electron Spectrosc. Relat. Phenom.* **166–7** 21–7